

Photonic band-gap engineering for volume plasmon polaritons in multiscale multilayer hyperbolic metamaterials

Sergei V. Zhukovsky,^{1,2,*} Alexey A. Orlov,² Viktoriia E. Babicheva,^{1,2,3} Andrei V. Lavrinenko,¹ and J. E. Sipe⁴

¹*DTU Fotonik – Department of Photonics Engineering, Technical University of Denmark, Ørsted Pl. 343, DK-2800 Kgs. Lyngby, Denmark*

²*National Research University of Information Technology,*

Mechanics and Optics, Kronverksky pr. 49, St. Petersburg, 197101, Russia

³*Birk Nanotechnology Center, Purdue University, 1205 West State Street, West Lafayette, IN, 47907-2057 USA*

⁴*Department of Physics and Institute for Optical Sciences, University of Toronto, 60 St. George Street, Toronto, Ontario, M5S 1A7, Canada.*

We theoretically study the propagation of large-wavevector waves (volume plasmon polaritons) in multilayer hyperbolic metamaterials with two levels of structuring. We show that when the parameters of a subwavelength metal-dielectric multilayer (“substructure”) are modulated (“superstructured”) on a larger, wavelength scale, the propagation of volume plasmon polaritons in the resulting *multiscale hyperbolic metamaterials* is subject to photonic band gap phenomena. A great degree of control over such plasmons can be exerted by varying the superstructure geometry. When this geometry is periodic, stop bands due to Bragg reflection form within the volume plasmonic band. When a cavity layer is introduced in an otherwise periodic superstructure, resonance peaks of the Fabry-Pérot nature are present within the stop bands. More complicated superstructure geometries are also considered. For example, fractal Cantor-like multiscale metamaterials are found to exhibit characteristic self-similar spectral signatures in the volume plasmonic band. Multiscale hyperbolic metamaterials are shown to be a promising platform for large-wavevector bulk plasmonic waves, whether they are considered for use as a new kind of information carrier or for far-field subwavelength imaging.

PACS numbers: 78.67.Pt, 81.05.Xj, 42.70.Qs, 73.20.Mf

I. INTRODUCTION

Metamaterials have attracted avid scientific interest over the last decade because optical materials with properties rare or absent in nature can be artificially engineered. Notable examples include media with negative refraction [1] or giant optical activity [2], and so-called indefinite media, which exhibit hyperbolic dispersion relations [3–6]. The latter are a special case of extreme anisotropy where components of the diagonalized permittivity tensor have opposite signs (e.g. $\epsilon = \text{diag}(\epsilon_x, \epsilon_y, \epsilon_z)$ with $\epsilon_x = \epsilon_y < 0$, $\epsilon_z > 0$ for uniaxial anisotropic media). With the introduction of these opposite signs, the dispersion relation,

$$\omega^2/c^2 = k_x^2/\epsilon_x + k_y^2/\epsilon_y + k_z^2/\epsilon_{x,y}, \quad (1)$$

changes from one of a conventional elliptical form to one of an “exotic” hyperbolic form (see Fig. 1a–b).

In the idealization that such a dispersion relation holds for all wavevectors, the isofrequency surface in the dispersion relation becomes unbounded (Fig. 1b). As a result, waves with very large wave vectors ($k^2 \gg \epsilon_{x,y,z} \omega^2/c^2$), which would normally be evanescent in any isotropic medium, can become propagating. Information carried by these “high- k modes” with anomalously small wavelength $2\pi/k$ can be used for far-field subwavelength imaging, as in the recent proposal of a hyperlens [7]. In addition, a multitude of high- k modes greatly increases the local photonic density of states (DOS) in

the indefinite medium, bringing about a variety of new physical effects including broadband spontaneous emission enhancement [8, 9], anomalous heat transfer beyond the Stefan-Boltzmann limit [10], and optical “tabletop simulation platform” for space-time phenomena such as metric signature transitions [11, 12].

Practical realization of indefinite media has been achieved over the past few years in the form of hyperbolic metamaterials (HMMs), which are highly anisotropic, subwavelength metal-dielectric composites. Two geometries of HMMs have

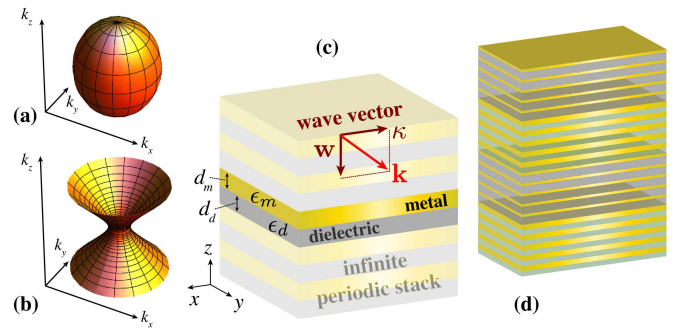


Figure 1. (Color online) Dispersion relation of (a) a conventional anisotropic medium ($\epsilon_{x,y,z} > 0$) with ellipsoidal isofrequency surface and (b) an indefinite medium ($\epsilon_{x,y} < 0$ and $\epsilon_z > 0$) with hyperboloidal isofrequency surface. (c) Schematic of a periodic metal-dielectric multilayer with wave vector decomposition $\mathbf{k} = w\hat{\mathbf{z}} + \kappa\hat{\mathbf{x}}$ used in Section II (schematic in that both w and κ can be complex). (d) Schematic example of a multiscale metal-dielectric HMM which is the main object of studies in this paper.

* sezh@fotonik.dtu.dk

been preferred so far due to their simplicity in both modeling and fabrication. They are (i) metallic nanorod arrays embedded in a dielectric host [13–15] and (ii) metal-dielectric multilayers [8, 9] shown in Fig. 1c. In both structures, the behavior expected for indefinite media was experimentally confirmed [8, 14], opening up many areas of theoretical and experimental research (see recent reviews [16, 17] and references therein). The finite size of the structure elements (rods or layers) puts an upper limit on the wave vectors k that still satisfy Eq. (1) [8, 18, 19]. Still, the existence of such waves in HMMs has been clearly demonstrated [20, 21]. Since these waves underlie the operation of a hyperlens and are crucial to other exotic physical properties of HMMs, it is very important to understand the physical nature of these waves and investigate the possible means of controlling their excitation and propagation.

The metal-dielectric composition of HMMs naturally leads one to suspect that high- k modes are plasmonic in nature. Even though the exact mechanism of their formation has been debated [22, 23], it is generally accepted that high- k propagating waves must originate from surface plasmon excitations at individual metal-dielectric boundaries [20]. Because of this, names such as *multilayer plasmons* [24], *Bloch plasmon polaritons* [20, 25], or *volume plasmon polaritons* (VPPs) [21] have been used by various groups. In our recent work [26], it was shown that VPPs originate from coupling between short-range surface plasmon polaritons in the individual metal layers.

In order to utilize the full potential of VPPs as subwavelength information carriers for hyperlensing and other applications, it is necessary to understand how these waves can be guided and otherwise manipulated. A remarkable thing to observe is that they are bulk propagating waves, so they should be subject to the photonic band-gap (PBG) effects similar to all other kinds of propagating waves. For an idealized model of homogeneous indefinite medium, a photonic structure can be imagined by imposing a modulation of medium parameters (e.g., $\epsilon_{x,y}$ and ϵ_z), with the PBG properties depending on the geometry of that modulation. For example, a periodic step-wise modulation is expected to act as a photonic crystal for VPPs. In a realistic multilayer HMM, one can similarly envisage adding a wavelength-scale “superstructure” to an HMM, which already has a subwavelength “substructure”. In such *multiscale HMMs*, schematically shown in Fig. 1d, VPP propagation is expected to be affected by the superstructure just as conventional light waves are controlled in photonic crystals. Just as unprecedented light control can be achieved in PBG structures, owing to a free choice of geometrical structures (e.g. periodic, coupled-cavity, quasiperiodic, fractal, etc.) and parameters, unprecedented control of plasmonic wave propagation should be possible by choosing an appropriate superstructure geometry in multiscale HMMs.

In this paper, we demonstrate this multiscale approach by proposing proof-of-concept designs of Bragg reflectors and Fabry-Pérot resonators for high- k bulk plasmons in multilayer metal-dielectric HMMs. Formation of PBGs in periodic multiscale multilayers is clearly seen in the numerically calculated Fresnel reflection coefficients in k -space. Breaking the period-

icity in the superstructure is shown to result in cavity resonant modes. Making the structure totally non-periodic increases the degree of freedom in using PBG effects to control the dispersion properties of HMMs. In particular, fractal multiscale HMMs are found to exhibit characteristic self-similar spectral features. Besides showing that high- k waves can be directly controlled by PBG effects, the proposed approach is useful in designing HMM-based devices to engineer and probe the spontaneous emission rate of nearby atoms in the evanescent-wave domain.

The paper is organized as follows. In Section II, we review the theoretical background on wave propagation in metal-dielectric multilayer HMMs, and discuss the dispersion relation of high- k VPP waves in such multilayers. In Section III, we introduce the concept of multiscale HMMs and show that VPPs can be manipulated by PBG effects. In particular, we demonstrate Bragg reflection and Fabry-Pérot resonances for VPPs in several periodic and nonperiodic multiscale geometries, including practically realizable designs. Finally, Section IV summarizes the paper.

II. VOLUME PLASMON POLARITONS IN MULTILAYER HYPERBOLIC METAMATERIALS

Consider a subwavelength periodic metal-dielectric multilayer as shown in Fig. 1c, where the permittivities of dielectric and metal are $\epsilon_d = \epsilon'_d + i\epsilon''_d$ ($\epsilon'_d > 0$) and $\epsilon_m = \epsilon'_m + i\epsilon''_m$ ($\epsilon'_m < 0$), respectively. The layer thicknesses are d_d for the dielectric and d_m for the metal, and $\rho \equiv d_m/(d_m + d_d)$ denotes the metal filling fraction.

Any plane wave existing in such a multilayer can have its wave vector \mathbf{k} represented as a sum of its in-plane component $\mathbf{\kappa} = k_x\hat{\mathbf{x}} + k_y\hat{\mathbf{y}}$, and its out-of-plane component $\mathbf{w} = \pm w\hat{\mathbf{z}}$. The former is constant across all layers due to the boundary conditions, so $\kappa = |\mathbf{\kappa}|$ can be conveniently used as a labeling parameter for the waves. The out-of-plane component can take the value $\pm w$ in each layer (denoted by the subscript m or d) with

$$w_{m,d} = \sqrt{\left(\frac{\omega}{c}\right)^2 \epsilon_{m,d} - \kappa^2}. \quad (2)$$

Generally we choose the square root of a complex number \sqrt{z} such that $\text{Im} \sqrt{z} > 0$, taking $\text{Re} \sqrt{z} \geq 0$ if $\text{Im} \sqrt{z} = 0$. Neglecting material absorption for now ($\epsilon''_{m,d} = 0$), we can see that w_d is real for $\kappa < \sqrt{\epsilon_d}\omega/c$, corresponding to propagating waves within the light cone for the dielectric layers, or purely imaginary otherwise, corresponding to evanescent waves outside the light cone. For metal layers below the plasma frequency, $\epsilon_m < 0$, so w_m is always imaginary.

If the layer thicknesses are subwavelength, the effective medium model is commonly used, and the entire multilayer is regarded as a homogeneous medium with the permittivity tensor $\hat{\epsilon}_{\text{eff}} = \text{diag}(\epsilon_x, \epsilon_y, \epsilon_z)$, where

$$\epsilon_x = \epsilon_y = \rho\epsilon_m + (1 - \rho)\epsilon_d, \quad \epsilon_z^{-1} = \rho\epsilon_m^{-1} + (1 - \rho)\epsilon_d^{-1}. \quad (3)$$

In such an extremely anisotropic medium, the expression for w of a p -polarized wave (for which surface plasmons can

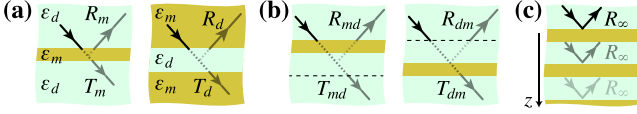


Figure 2. (Color online) Illustration of the Fresnel reflection and transmission coefficient derivation: (a) for a single metal or dielectric layers as in Eq. (7); (b) for a metal-dielectric bilayer as in Eq. (10); (c) for a semi-infinite periodic metal-dielectric multilayer as in Eq. (11).

propagate along metal-dielectric interfaces) is [27]

$$w_{\text{eff}} = \sqrt{\left(\frac{\omega}{c}\right)^2 \epsilon_x - \frac{\epsilon_x}{\epsilon_z} \kappa^2}. \quad (4)$$

For layered HMMs it is typical that $\epsilon_x < 0$ and $\epsilon_z > 0$ (again, neglecting absorption for the moment). Then, we see that the second term under the square root in Eq. (4) becomes negative and overrules the first term for large enough κ . So the entire expression under the root becomes positive. Thus, the waves change from evanescent (imaginary w) to propagating (real w) at $\kappa = \kappa_c$ defined as $w_{\text{eff}}(\kappa_c) = 0$.

Continuing to neglect absorption, we consider the expression of the Fresnel reflection coefficient for a boundary between a homogeneous dielectric and a medium described by the permittivity tensor in Eq. (3) [26],

$$R_{\text{eff}} = \frac{w_d \epsilon_x - w_{\text{eff}} \epsilon_d}{w_d \epsilon_x + w_{\text{eff}} \epsilon_d}. \quad (5)$$

In the region of large real κ , for which w_d is imaginary, we see that real (rather than imaginary) w_{eff} causes R_{eff} to acquire a non-vanishing imaginary part [28]. In other words, $\text{Im} R_{\text{eff}}(\kappa)$ is non-zero for those values of κ that correspond to propagating waves in the effective medium.

This correspondence is physically significant, and can be extended to the case of actual multilayers. On the one hand, the dispersion relation of propagating Bloch waves in an infinite periodic metal-dielectric multilayer can be determined from the transfer matrix method [29]. The transfer matrix of one period can be written as

$$M_1 = \frac{1}{T_m} \begin{bmatrix} T_m^2 - R_m^2 & R_m \\ -R_m & 1 \end{bmatrix} \begin{bmatrix} e^{i w_d d_d} & 0 \\ 0 & e^{-i w_d d_d} \end{bmatrix}, \quad (6)$$

where the reflection and transmission coefficients of a metal layer (see Fig. 2a) are given by the Airy formulas,

$$R_m = r_{dm} + \frac{t_{dm} r_{md} t_{md} e^{2i w_m d_m}}{1 - r_{md}^2 e^{2i w_m d_m}}, \quad T_m = \frac{t_{dm} t_{md} e^{i w_m d_m}}{1 - r_{md}^2 e^{2i w_m d_m}}; \quad (7)$$

the coefficients $r_{dm,md}$ and $t_{dm,md}$ are the interface coefficients for p -polarized waves determined by the Fresnel formulas,

$$\begin{aligned} r_{md} &= \frac{w_m \epsilon_d - w_d \epsilon_m}{w_m \epsilon_d + w_d \epsilon_m}, & r_{dm} &= \frac{w_d \epsilon_m - w_m \epsilon_d}{w_d \epsilon_m + w_m \epsilon_d}; \\ t_{md} &= \frac{2 w_m \sqrt{\epsilon_m \epsilon_d}}{w_m \epsilon_d + w_d \epsilon_m}, & t_{dm} &= \frac{2 w_d \sqrt{\epsilon_d \epsilon_m}}{w_d \epsilon_m + w_m \epsilon_d}. \end{aligned} \quad (8)$$

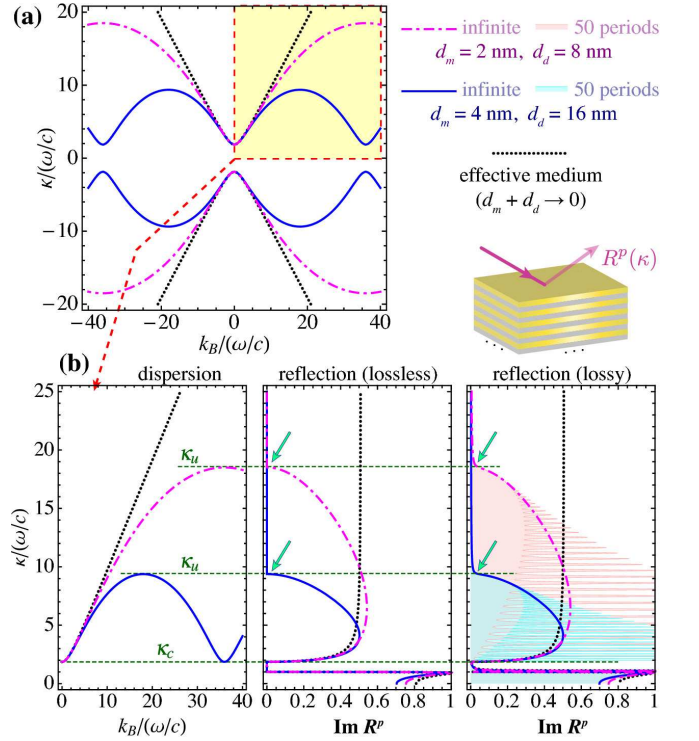


Figure 3. (Color online) (a) Dispersion relation for high- k Bloch waves in an infinite metal-dielectric HMM comprising alternating Ag/epoxy layers ($\epsilon_m = -30.1 + i\epsilon_m''$, $\epsilon_d = 2.72$ for $\lambda = 720$ nm [30]) with $\rho = 0.2$ and different layer thicknesses. (b) An enlarged view of a part of that dispersion relation along with the imaginary part of the Fresnel reflection coefficient, $\text{Im} R^p$, for a semi-infinite effective multilayer (see inset) without losses ($\epsilon_m'' = 0$) and with losses ($\epsilon_m'' = 0.41$) [28]. The dotted lines denote the limiting case of the homogeneous effective anisotropic medium [Eq. (3)], corresponding to a multilayer with infinitely thin layers. The horizontal dashed lines denote the VPP band edges, and faint green arrows highlight the differences in $\text{Im} R^p$ for lossless vs. real metal. The shaded areas in the rightmost plot correspond to a finite (50-period) multilayer as opposed to an infinite one.

and $w_{m,d}$ are given by Eq. (2). According to Bloch's theorem, the normal wave vector component k_B of the propagating Bloch wave with tangential wave vector component κ ($k^2 = k_B^2 + \kappa^2$) is determined as $\cos[k_B(d_m + d_d)] = (\text{Tr} M_1)/2$, resulting in a well-known dispersion relation [22, 23, 30]

$$\begin{aligned} \cos[k_B(d_m + d_d)] &= \cos(w_m d_m) \cos(w_d d_d) \\ &- \frac{1}{2} \left(\frac{\epsilon_m w_d}{\epsilon_d w_m} + \frac{\epsilon_d w_m}{\epsilon_m w_d} \right) \sin(w_m d_m) \sin(w_d d_d). \end{aligned} \quad (9)$$

The solution of this equation in the wave vector space defines a band of propagating high- k VPP waves (see Fig. 3a), which exists within certain limits $\kappa_c < \kappa < \kappa_u$. The lower band edge κ_c is determined by the above mentioned condition $w_{\text{eff}}(\kappa_c) = 0$, and coincides with the prediction of the effective medium theory. Conversely, the upper band edge $\kappa_u \propto (d_m + d_d)^{-1}$ is associated with the breakdown of that approximation due to the finite layer thickness [28].

On the other hand, the reflection coefficient of a semi-infinite multilayer HMM can also be analytically determined. Applying the Airy formulas (7) one more time to a stack of two layers (metal and dielectric, see Fig. 2b) lets us express the transmission and reflection of such bilayers in terms of the single-layer reflection and transmission coefficients as [31]

$$R_{md} = R_m, \quad R_{dm} = R_m e^{2i w_d d_d}, \quad T_{md} = T_{dm} = T_m e^{i w_d d_d}, \quad (10)$$

with R_m and T_m given by Eq. (7). Since a semi-infinite structure remains unchanged when its outermost period is removed, its reflection coefficient R_∞ must satisfy a quadratic equation

$$R_\infty = R_{md} + \frac{T_{md} R_\infty T_{dm}}{1 - R_\infty R_{dm}}. \quad (11)$$

Solving this equation and choosing the solution for which the wave would be decaying, rather than growing, as z increases (see Fig. 2c) we can determine R_∞ [32].

In the absence of losses and for $\kappa > (\omega/c)\sqrt{\epsilon_d}$, we can see that $w_{m,d}$ are purely imaginary, and consequently, $R_{md,dm}$ and $T_{md,dm}$ are purely real [see Eqs. (7)–(8)]. Then it can be shown that the existence condition for VPPs in the form $|\text{Tr} M_1| \leq 2$ coincides with the condition $\mathcal{D} \leq 0$, where \mathcal{D} is the discriminant of the quadratic equation (11), ensuring that its roots become complex even though its coefficients are real. This generalizes the relation between non-zero imaginary part of the reflection coefficient at an interface and the existence of propagating waves beyond the interface in the evanescent-wave domain from the case of a single interface (as seen in Eqs. (4)–(5) above and as elaborated in Appendix A) to the case of a semi-infinite periodic multilayer HMM. Namely, we find that the imaginary part of R_∞ is non-zero within the VPP band found by Bloch’s theorem. Indeed, Fig. 3b shows that the range where $\text{Im} R_\infty \neq 0$ is exactly $\kappa_c < \kappa < \kappa_u$, where propagating high- k VPP waves were shown to exist. Elsewhere in the high- κ range, $\text{Im} R_\infty = 0$ and no propagating solutions are allowed.

Even though rigorously derived for lossless, semi-infinite multilayers, this criterion is still a useful one if losses are present ($\epsilon''_{m,d} \neq 0$). Figure 3b shows that the abrupt appearance of non-zero $\text{Im} R_\infty$ at the band edges is smeared [28] because the sharp distinction between evanescent and propagating waves can no longer be made if the materials are lossy. However, the general argument still persists that $\text{Im} R_\infty$ is significantly non-zero when the Bloch solutions of the dispersion equation are propagating.

Moreover, including losses makes it possible to generalize the relation between non-zero $\text{Im} R_\infty$ and the existence of propagating waves inside a finite multilayer structure. Note first that for lossless *finite* multilayer structures with $\kappa > (\omega/c)\sqrt{\epsilon_d}$ we see that all quantities entering the transfer matrix M_1 are real. Hence, the reflection coefficient of such a multilayer structure must be real, too, with the exception of a discrete set of poles where the reflection coefficient diverges and its phase becomes indeterminate; these poles are known to signify the presence of guided modes inside the multilayer. As the number of layers in the structure increases, the number of poles grows accordingly, but it is only in the limit of an

infinite multilayer that the transition from a discrete set to a continuous band can occur, as shown above. When it occurs, modes that are guided along the layers in a finite multilayer acquire a real z -component of the wave vector [k_B as given by Eq. (9)] and become propagating “through the bulk” of an infinite multilayer; it is for this reason that we refer to these waves as *volume* plasmon polaritons.

Thus, in the truly lossless case, finite multilayers only support surface waves with a discrete set of $\kappa > (\omega/c)\sqrt{\epsilon_d}$, whereas infinite multilayers can additionally support bulk propagating waves (VPPs) in a continuous range of κ . However, the presence of losses (even very minor ones) regularizes this opposition, transforming each discrete point into a narrow peak where $\text{Im} R(\kappa) \neq 0$. When there are many layers in the structure, some of these peaks typically merge into a continuous band (see Fig. 3b), which is seen to approach the dependence $\text{Im} R_\infty(\kappa)$ as the number of layers increases. Within this VPP band, there are waves inside the multilayer HMM that are quasi-propagating in the sense that (i) their propagating character is primarily determined by the infinite-structure dispersion relation and is only weakly influenced by the number of layers in the structure, (ii) they undergo a much weaker attenuation than they would undergo in any homogeneous isotropic medium, and (iii) they become less attenuated if losses are lowered. In contrast, waves outside the VPP band remain strongly evanescent regardless of whether material losses are present.

Hence we will be using the existence of $\text{Im}[R(\kappa)]$ as a “footprint,” providing evidence for the existence of high- k waves, or VPPs, in a range of HMM multilayer structures.

III. MULTISCALE HYPERBOLIC METAMATERIALS

Since VPPs are bulk Bloch plasmonic waves with propagating character, they have to be subject to the PBG effects just as any other kind of propagating waves. A straightforward idea is to apply these PBG effects to modulate the properties of a subwavelength multilayer HMM (in particular, the metal filling fraction ρ) on a larger length scale (Fig. 1d). To distinguish the two scales, we will refer to the coarser, wavelength-scale modulation as the “superstructure” consisting of several *superlayers*; Fig. 4a displays two kinds of such superlayers (denoted A and B) with thicknesses $D_{A,B}$ and filling fraction $\rho_{A,B}$, respectively. The finer subwavelength periodic metal-dielectric structure within each superlayer, which gives rise to HMM properties, is called the “substructure”. Thus, each superlayer contains a certain number of subperiods, $N_{A,B} = D_{A,B}/(d_m + d_d)$, or twice as many *sublayers*.

The resulting multiscale multilayer is expected to exert the same degree of control over VPP waves as the corresponding photonic multilayers control propagation of conventional electromagnetic waves. Hence, a periodic arrangement of superlayers, where the layers denoted by A and B simply alternate, should result in a band gap for VPPs. In a further analogy with photonic multilayers, this band gap should forbid the propagation of waves with values of κ around a certain mid-gap value κ_0 , for which the superlayers are close to be quarter-

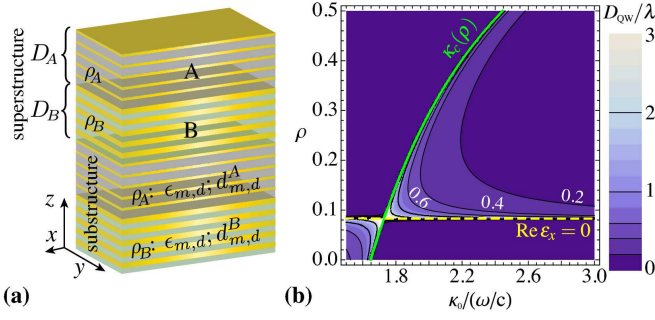


Figure 4. (Color online) (a) Schematics of a multiscale HMM with periodic geometry, showing the division into superstructure and substructure. (b) Dependence of the QW layer thickness D_{QW}/λ on filling fraction ρ and the target PBG location κ_0 according to Eq. (12). The solid green line denotes the lower VPP band edge $\kappa_c(\rho)$, and the dashed yellow line marks the boundary of the HMM regime ($\text{Re}[\epsilon_x] = 0$).

wave (QW), i.e., their optical thickness should be close to one quarter of the wavelength that corresponds to $w_{\text{eff}}(\kappa_0)$. In the remainder of this section, we will investigate the influence of the superstructure geometry on the VPP propagation in a variety of multiscale HMMs.

A. Bragg reflectors and Fabry-Pérot resonators with thick-layer superstructure

In order to demonstrate the multiscale concept, we will first consider structures where the superstructure and substructure length scales are clearly separated, i.e., $\lambda/4 \simeq D_{A,B} \gg d_{m,d}$ (or $N_{A,B} \gg 1$). Keeping in mind that the wavelength of high- k VPPs, $\lambda \simeq 2\pi/k$, can be anomalously small compared to the vacuum wavelength $\lambda_0 = \omega/c$, it can be expected that the target κ_0 should be no more than several times larger than ω/c . To overcome this apparent contradiction, we determine the thickness D_{QW} of a “model” homogeneous QW layer made of the effective medium [see Eq. (3)] for a given κ_0 . From Eq. (4),

$$D_{\text{QW}} = \frac{\lambda}{4} \left(\text{Re} \left[\sqrt{\frac{\omega^2}{c^2} \epsilon_x - \frac{\epsilon_x}{\epsilon_z} \kappa_0^2} \right] \right)^{-1} \quad (12)$$

The dependence of D_{QW} on ρ and κ_0 is shown in Fig. 4b. It is seen that to be able to form a PBG well into the high- κ range and still have a clear separation of length scales ($D_{\text{QW}} \gg d_{m,d}$), one should use filling fractions slightly above 0.08, for which $\epsilon_x \lesssim 0$. Otherwise, we see that $D_{\text{QW}} \ll \lambda$ unless κ_0 is very close to the lower VPP band edge ($\kappa \gtrsim \kappa_c$).

Therefore, the design of a Bragg reflector for VPPs involves choosing two values of ρ for the superlayers (ρ_A and ρ_B), and then using Eq. (12) to determine the superlayer thicknesses $D_{A,B}$. Following the example of Ni *et al.* [30], and choosing silver and epoxy as metal and dielectric materials, respectively ($\epsilon_m = -30.1 + 0.41i$, $\epsilon_d = 2.72$ for $\lambda = 720$ nm), we choose $\rho_A = 0.1$ and $\rho_B = 0.14$. To form a band gap at a target

$\kappa_0 = 4\omega/c$, we arrive at $D_A = 116.4$ nm and $D_B = 65.8$ nm, approximately corresponding to $N_A = 29$ and $N_B = 16$ metal-dielectric bilayers with $d_m + d_d = 4$ nm thickness (Fig. 5a).

Such layers would be very difficult to fabricate, and are so thin that it is unlikely bulk optical constants could be used to characterize them. Nonetheless, as an initial analysis we theoretically characterize these nominal structures (Fig. 5b–g) to help identify some of the essential physics. Considering first the semi-infinite superstructure ($M = 10^4$ periods in practical calculations) to suppress pass-band states, and artificially lowering the imaginary part of the metal permittivity to 10% of its actual value, we clearly see a range of very low $\text{Im}R$ around the target midgap $\kappa_0 = 4\omega/c$ (Fig. 5b), signifying inhibited VPP propagation as described in Section II above. This range, or stop band, is seen to widen as the modulation depth of the filling fraction ρ increases, which is characteristic of a PBG opening and confirms that VPPs indeed undergo Bragg reflection in a periodic-superstructure multiscale HMM.

Restoring the amount of losses in metal to their actual value (Fig. 5c), we see that the band gap is less pronounced but nevertheless quite visible. Compensating the loss in silver by incorporating optical gain in the dielectric layers of the HMM (putting $\epsilon_d = 2.72 - 0.04i$, as was recently envisaged by Ni *et al.* [30]) restores the pronounced character of the band gap (see Fig. 5d). The effects of loss and gain on the band gap visibility are additionally highlighted in Fig. 5e–f where it is shown that adding gain to the dielectric layers indeed results in partial loss compensation. Since the working filling fractions are around 0.1, so that $d_d \approx 10d_m$, the negative imaginary component of ϵ_d in the range of 0.04 is sufficient to compensate the loss in silver corresponding to $\epsilon_m'' = 0.41$. Indeed, the inset in Fig. 5f demonstrates that the gap profile for the gain-compensated HMM is almost identical with that for the structure where loss is artificially reduced to 10%. Finally, Fig. 5g shows that reducing the number of superperiods does not change the location of the stop band for VPPs but strongly modifies the propagation of such waves in the surrounding “pass band” of the high- κ range, featuring multiple band edge-like resonances.

Stacking a periodic Bragg reflector with its mirror image forms a structure with geometry ABAB...ABBA...ABAB (Fig. 6a), creating a half-wave defect or cavity (“BB”) in an otherwise periodic structure. By analogy with photonic multilayers, such a structure should function as a Fabry-Pérot resonator for VPPs, creating a narrow band of $\kappa \approx \kappa_{\text{res}}$ where the plasmon energy gets trapped in the cavity and the waves can tunnel through the structure despite the presence of a band gap. This feature should be observed as a sharp peak of $\text{Im}[R(\kappa_{\text{res}})]$ inside the forbidden gap. Varying the thickness of the cavity layer (by adjusting the number of subperiods in it), it should be possible to tune the location of κ_{res} across the band gap.

Such behaviour is indeed observed in Fig. 6. The peak location is seen to shift as additional substructure periods are removed from or added to the defect layer, varying its thickness (Fig. 6b). Note the stark contrast between the marked shift of the central resonance peak and nearly absent shift of the remaining resonances in the wavevector spectra. This means

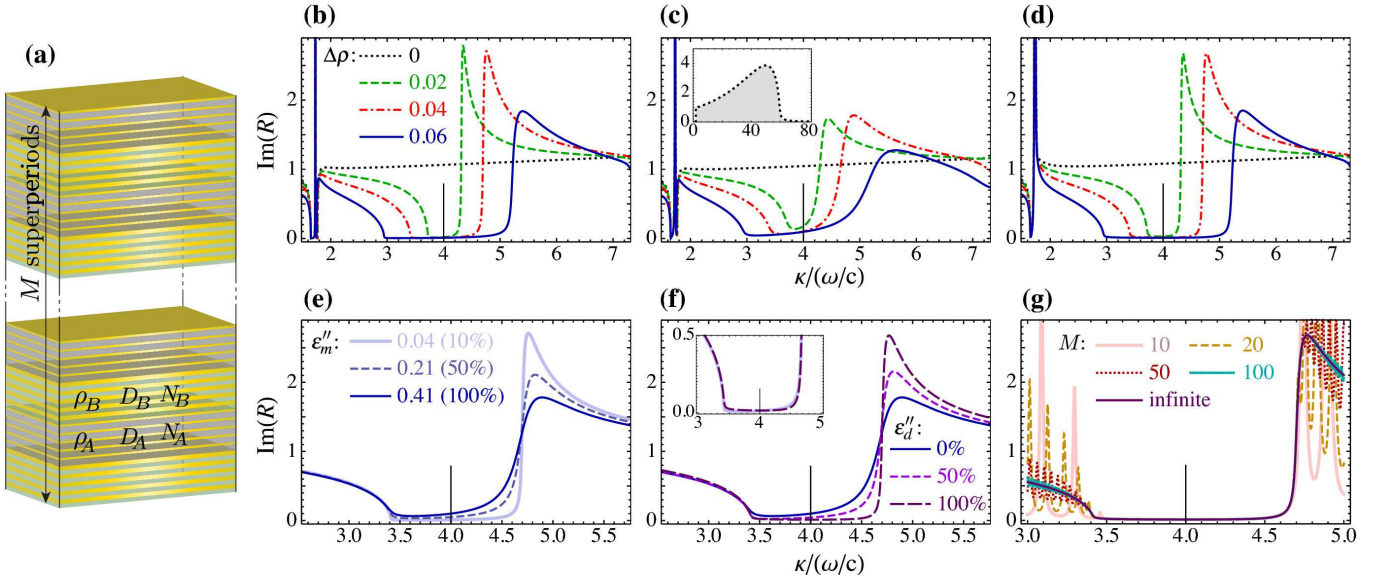


Figure 5. (Color online) Characterization of a multiscale Bragg reflector for high- k waves shown schematically in (a) with the default geometry comprising a superstructure with $M = 10^4$ periods of HMM layers with $(\rho_A + \rho_B)/2 = 0.12$, the substructure period $d_m + d_d = 4$ nm, and superlayer thickness $N_{A,B}$ determined from Eq. (12). *Top row*: the function $\text{Im}[R(\kappa)]$ for a varying depth of superstructure modulation ($\Delta\rho = \rho_A - \rho_B$) for (b) 10% losses in silver ($\epsilon_m'' = 0.04$), (c) full losses in silver ($\epsilon_m'' = 0.41$), and (d) full losses in silver compensated by gain in the epoxy layers as described in [30] ($\epsilon_m'' = 0.41$ and $\epsilon_d'' = -0.04$); the dotted line shows the structure with no superstructure ($\rho_A = \rho_B = 0.12$), with the full high- κ band shown in the inset of (c). *Bottom row*: the dependence of $\text{Im}[R(\kappa)]$ for the structure with $\rho_A = 0.1$, $\rho_B = 0.14$ and $N_A = 29$, $N_B = 16$ near the gap region (e) for varying amount of loss in silver ϵ_m'' for $\epsilon_d'' = 0$, (f) for varying amount of gain in dielectric ϵ_d'' for $\epsilon_m'' = 0.41$, and (g) for a varying number of superperiods M . The inset in (f) compares the cases of 10% losses without gain and 100% losses with gain.

that the central peak is a Fabry-Pérot resonance whereas the remaining peaks are not related to the cavity layer. For VPPs corresponding to the Fabry-Pérot resonance, it can be concluded that they are localized in the defect and guided within the x - y plane.

Note that a much smaller number of periods in the superstructure is necessary for the appearance of the resonance peak than for the appearance of the band gap (see Fig. 5). For a larger number of periods in the superstructure it is seen that the guided high- k VPP waves decouple from the incident wave, making them harder to characterize or interact with (Fig. 6c). Also, similar to what we could see in Fig. 5, absorption in metal is highly detrimental: without compensation, the resonance peaks all but vanish when the imaginary part of ϵ_m reaches 10% of its actual value. However, in presence of gain the peaks are seen to reappear even with full metal losses (Fig. 6d); the peaks are notably broadened but their location is not affected (see the inset in Fig. 6b).

B. Bragg reflectors and Fabry-Pérot resonators with thin-layer superstructure

The approach of the previous subsection has a didactic advantage, with its easy separation of superstructure and substructure length scales; this makes the multiscale features that arise easy to understand. However, structures with $d_m + d_d = 4$ nm, and indeed with $d_m \simeq 0.5$ nm, cannot be easily fabri-

cated and, even if they could, the optical response of such thin layers would not likely be described by bulk dielectric constants. Further, even were fabrication possible it was shown that absorption is very detrimental to PBG effects, requiring either low-loss plasmonic materials [33] or loss compensation means [30] for the effects to be observed. These disadvantages are worsened by the need for structures consisting of hundreds (if not thousands) of sublayers, leading even the most optimistic to despair of fabrication at any time in the near future. As a result, thick-superlayer structures for VPPs in multilayer HMMs can only be considered as proof-of-concept structures, and are not viable from a practical point of view.

To alleviate these fabrication challenges, we consider here the other extreme of the multiscale concept and analyze the structures where superlayers consist of just one subperiod ($N_A = N_B = 1$), allowing the metal and dielectric sublayers to be only moderately thin. In this regime, the subwavelength approximations will certainly fail [28], so Eq. (12) can no longer be regarded as an accurate prediction of a QW layer thickness. Instead, the structure can be considered as a periodic multilayer with a more complicated unit cell containing four layers (a double-periodic structure, see Fig. 7a). Calculating its transfer matrix in a similar manner to Eq. (6) and applying Bloch's theorem along the lines of Section II, one can obtain the high- k dispersion relation of such a double-periodic structure with infinite number of periods. One can see (Fig. 7b) that if the filling fraction difference $\Delta\rho = \rho_A - \rho_B$ is non-zero, the VPP band splits into two, leaving a gap between them, which

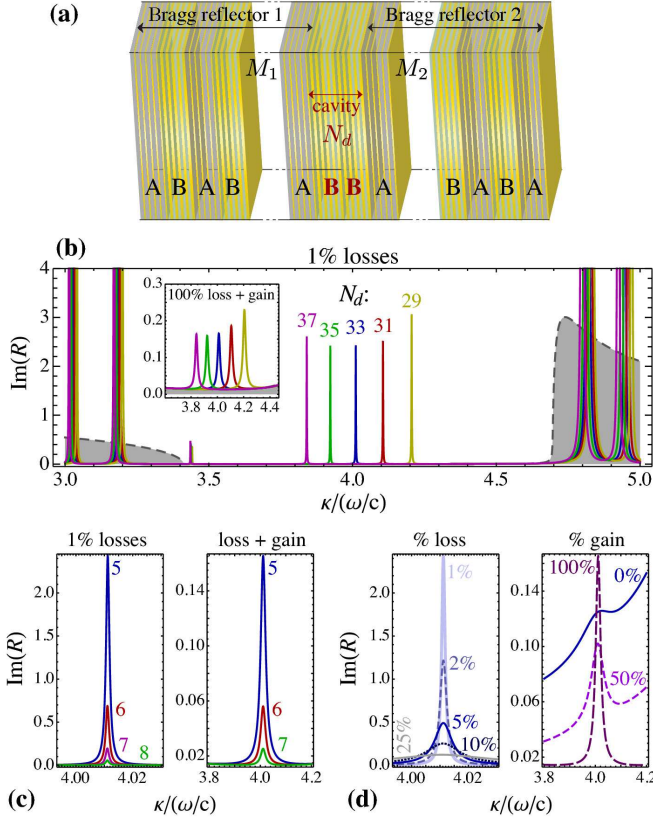


Figure 6. (Color online) Characterization of a multiscale Fabry-Pérot resonator for VPPs. (a) Schematics of the structure. (b) Dependence $\text{Im}[R(\kappa)]$ for different thickness of the defect layer expressed in the number of superperiods N_d for a superstructure with the same parameters as in Fig. 5 but with $M_1 = M_2 = 5$ and 1% losses ($\epsilon_m'' = 0.004$); the inset shows the excerpt of the same dependence for full losses in metal compensated by gain in the dielectric ($\epsilon_m'' = 0.41$ and $\epsilon_d'' = -0.04$). Also shown are the enlarged views of the cavity resonance peak under varying conditions in structures with (c) varying number of superperiods $M_1 = M_2$ and (d) varying degree of loss and gain in the constituent materials.

widens as $\Delta\rho$ increases. Since we are no longer restricted by the condition $D_{A,B} \gg d_{m,d}$, we can consider a structure with thicker sublayers (e.g., $d_m + d_d = 20$ nm), which would be far more realistic for fabrication. We are also free to work with a greater contrast of ρ , and, as seen in Fig. 7b, a prominently wide band gap can be achieved for an example structure with $\rho_A = 0.60$ and $\rho_B = 0.34$. The gap location is now in the higher- κ part of the wavevector space, around $\kappa \simeq 5 \dots 7\omega/c$, and it turns out that Eq. (12) is still able to give a meaningful estimate of the gap location, predicting the mid-gap κ to be $6.75\omega/c$.

Figure 7c–d shows the characterization of such a multiscale HMM with different number of superperiods. We can see that a PBG for VPPs does form at the predicted location with clear separation between pass bands and stop bands with as few as several tens of superlayers. Together with practically achievable values for the sublayer thicknesses, this makes the whole structure much more promising for experimental realization

than the thick-superlayer counterparts. Finally, it can be seen that the PBG is still clearly pronounced with the realistic account for the losses in silver (Fig. 7c). To make sure that the feature seen in Fig. 7c is actually a PBG for VPPs seen in Fig. 7b, we compare the electric field distribution at three different κ , namely, below, inside, and above the band gap (Fig. 7e). The field distribution shows the evanescent vs. extended character of the waves inside the HMM for κ inside vs. outside of the band gap, respectively.

By adding gain to the dielectric layers, the gap becomes even more clearly defined, approaching abrupt band edges characteristic for the lossless case (see Fig. 3b). This near-total loss compensation makes this structure a practically realizable candidate for a Fabry-Pérot resonator for VPPs. As before, a basic half-wave defect is formed by repeating one of superlayers twice, or simpler, by stacking a 3-superperiod structure (ABABAB) with its mirror image (BABABA), as seen in Fig. 8a. Rather than varying the number of sublayers in the cavity region (which is not possible since $N_A = N_B = 1$ and $N_d = 2$), the resonance location can be tuned by adjusting the thickness of one of the metal layers in the cavity region. Indeed, the characterization in Fig. 8b shows the possibility of moving the VPP resonance peak across the band gap. The field distribution calculations show that when κ matches the peak in the dependence $\text{Im}R(\kappa)$, the structure features a Fabry-Pérot resonant mode localized near the cavity layer, whereas elsewhere in the band gap the waves in the HMM remain evanescent.

Figure 8c shows the dependence of the peak profile on the number of superperiods in the Bragg mirrors surrounding the cavity. As before, increasing this number beyond 4 makes the peak vanish by decoupling the localized VPP mode from the incident wave, and reducing the amount of gain leads to broadening of the peak, again to the point of vanishing, due to the decrease in its Q -factor.

Overall, we see that thin-superlayer multiscale HMMs can exert the same PBG behavior on VPPs as their thick-superlayer counterparts, but with a much smaller number of moderately thin layers, making such structures much more feasible for experimental realization. As a price to pay, the gap and/or resonance position can no longer be smoothly tuned by varying the number of subperiods in the superstructure; other methods such as departing from the QW condition in selected layers have to be used instead. We also see that for this thin-superlayer structure the gain compensation is quite successful in increasing the visibility of PBG effects. However, we refrain from far-reaching conclusions based on this result because the behavior of VPPs in presence of gain strong enough to fully compensate (or even overcompensate) losses needs further investigation.

C. Multi-gap and fractal Cantor multiscale HMMs

As a final example, we briefly touch upon the possibility of band gap engineering for VPP by using more complicated superstructure geometries than simple periodicity. Note that doubling the number of subperiods in some superlay-

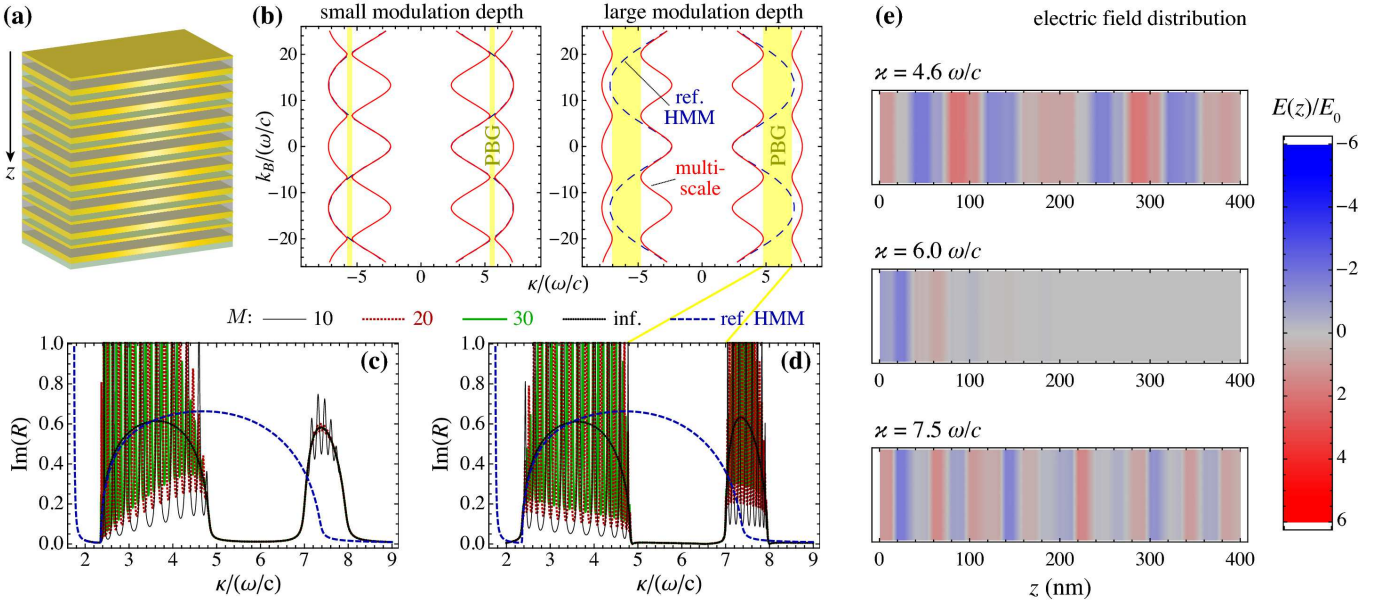


Figure 7. (Color online) Characterization of a Bragg reflector for high- k waves comprising a superstructure of 10 to 30 layers, each consisting of one subperiod ($N_A = N_B = 1$) with $\rho_A = 0.60$, $\rho_B = 0.34$, and $d_m + d_d = 20$ nm. (a) Schematic of the structure; (b) Dispersion relation similar to Fig. 3 for an infinite double-periodic structure for small and large filling fraction modulation $\Delta\rho$. (c–d) $\text{Im}R(\kappa)$ for full metal losses (c) without and (d) with gain in the dielectric. The dashed line shows the reference VPP band from a HMM with average $\rho_A = \rho_B = 0.473$. (e) Electric field distribution in the structure with 20 periods for $\kappa c/\omega$ equal to 4.6 (below the band gap); 6.0 (inside the band gap); 7.5 (above the band gap).

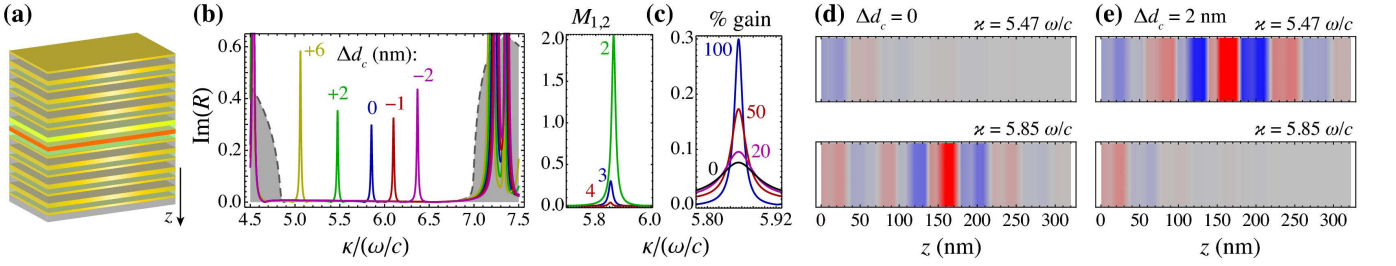


Figure 8. (Color online) Characterization of a Fabry-Pérot resonator for high- k waves comprising a superstructure with $M_1 = M_2 = 3$ periods of two superlayers with same substructure as in Fig. 7. (a) Schematic of the structure, highlighting the cavity region and variable-thickness metal layer in it; (b) $\text{Im}R(\kappa)$ in presence of gain for varying thickness of the central metal layer, Δd_c being the thickness adjustment compared to the ideal half-wave defect; (c) $\text{Im}R(\kappa)$ for 100% of metal losses and gain compensation in the dielectric. (c) Enlarged view of the peak for varying number of superperiods and degree of gain. The pictures at the bottom show the field distribution in the structures with (d) $\Delta d_c = 0$ and (e) $\Delta d_c = 2$ nm: top plots, $\kappa = 5.47\omega/c$ (on-peak for $\Delta d_c = 2$ nm); bottom plots, $\kappa = 5.85\omega/c$ (on-peak for $\Delta d_c = 0$). The color scale is the same as in Fig. 7e.

ers of thin-superlayer structures (changing from $N_{A,B} = 1$ to $N_{A,B} = 2$) drastically influences the corresponding layers: they transform from quarter-wave-like to half-wave-like. This is expected to result in band gap splitting. Indeed, Fig. 9 shows that by simple alteration of the superstructure periodicity, this multi-gap multiscale HMMs can be realized. Aside from providing more versatility in the control over high- k wave propagation, this effect allows to push the band gap to the region with lower κ , which are easier to excite and which are more prevalent in the emission of a realistic source (finite-sized and/or located at a finite distance from the HMM [18, 34]).

We can also envisage multiscale HMMs where superlayers lose their periodicity entirely, while maintaining their long-

range order, i.e., an ordered non-periodic superstructure. Out of the many examples of such non-periodic geometries [35], we will focus on a fractal Cantor-like structure [36–38]. These structures are known for scalable and self-similar features in their optical spectra closely related to their geometry [38–40].

Specifically, we will consider the simplest middle-third Cantor sequence (Fig. 10a), described by the inflation rules

$$A \rightarrow AAA, \quad B \rightarrow BAB, \quad (13)$$

applied to a single layer of the type B (the “seed”) several times to form the Cantor structure of a given number of gen-

eration. This procedure yields the following sequence:

$$\begin{aligned} C_0 &= B, \quad C_1 = BAB, \quad C_2 = BABAAABAB, \\ C_3 &= BABAAABABAAAAAABABAAABAB. \end{aligned} \quad (14)$$

It can also be written as a recurrent relation,

$$C_{n+1} = C_n (A)^{3^n} C_n, \quad (15)$$

which underlies its geometrical self-similarity and gives rise to self-similar features in the optical spectra (Fig. 10a) [39].

Using the substructure geometry similar to the previous cases as the building blocks for A- and B-layers in Eqs. (13)–(15), we analyze the fractal multiscale HMMs corresponding to the second- and third-generation Cantor structures (containing 9 and 27 superlayers, respectively). The results are shown in Fig. 10b–c. It can be seen that characteristic scalable signatures of the Cantor spectra can be observed for VPPs in the high- κ region of the wave vector space. These features are distorted compared to the traditional fractal multilayers because of the non-QW nature of the sublayers involved. Nonetheless, they are observed in a realistic structure with metal losses taken into account. So, we can expect that known relations between geometrical and optical properties in deterministic non-periodic multilayers should also be manifest in HMMs with corresponding superstructure geometry. As a result, we can make use of the extensive knowledge of PBG properties of multilayers [37] to be able to control VPP propagation in multiscale HMMs with significant freedom.

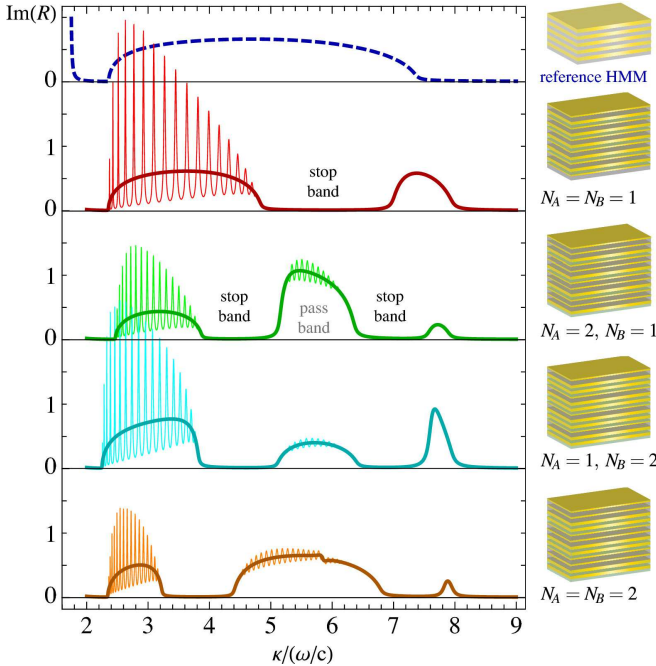


Figure 9. (Color online) Schematics and high- k band characterization of the structure with $N_A = N_B = 1$ vs. structures with doubled number of subperiods ($N_A = 2, N_B = 1$; $N_A = 1, N_B = 2$; $N_A = N_B = 2$) with $M = 20$ superperiods. Other parameters are the same as in Fig. 7. Full metal losses are considered.

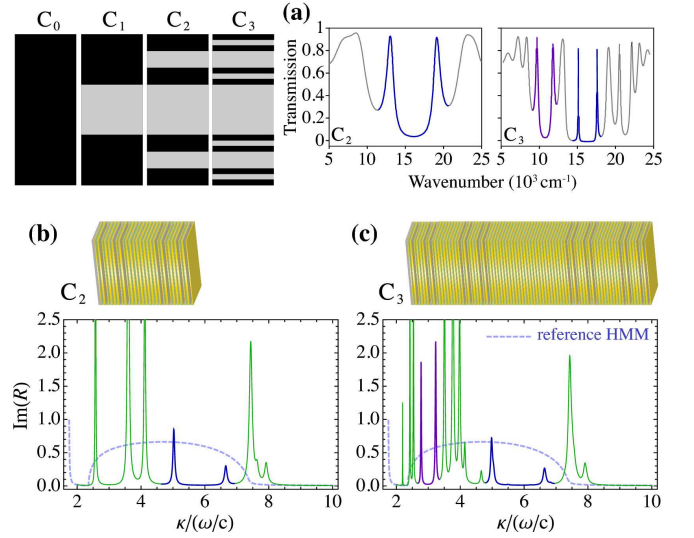


Figure 10. (Color online) (a) Schematics of middle-third Cantor section algorithm and an example of the optical spectrum of a Cantor multilayer [38, 39]. (b) Schematics and high- k band characterization of a second-generation Cantor structure (C_2 , 9 superlayers). (c) Same as (b) but for the third-generation Cantor structure (C_3 , 27 superlayers). The substructure geometry is the same as in Fig. 7. Full metal losses are considered.

IV. CONCLUSIONS

To summarize, we have demonstrated that a multiscale approach can be used to control large-wavevector, bulk plasmonic waves (volume plasmon polaritons) in multilayer metal-dielectric HMMs. As a proof of concept, we have proposed the design of Bragg reflectors and Fabry-Pérot resonators for these VPP waves. The designs consists of two levels of structuring: (i) a substructure of subwavelength metal and dielectric layers, responsible for creating hyperbolic dispersion, and (ii) a superstructure, which constitutes wavelength-scale variation of metal filling fraction and exerts PBG effects on VPPs. Band gaps and resonances for VPPs have been demonstrated by examining the Fresnel reflection coefficient in the large-wavevector region. More complicated superstructure geometries such, as fractal Cantor-like multiscale HMMs, have also been studied.

Along with proof-of-concept designs involving very large numbers of layers, more realistic thin-superstructure designs have been proposed, containing several tens of layers with thickness on the order of 10 nm, which is within reach of modern fabrication technology. It has also been shown that mechanisms to mitigate material absorption, for example introducing gain-based compensation in dielectric layers [30], make PBG effects more pronounced in all of the considered structures.

Our results show that VPPs can be directly controlled by the PBG effects, which may be enabling for employing VPPs to transmit optical signals. Using a great variety of superstructure geometries in the proposed multiscale approach is promising in the design of HMM-based devices with pre-

determined wavevector-space distribution of bulk plasmonic waves. Such devices can be used in hyperlenses with tailored properties, as well as to probe and tailor light-matter interaction phenomena of nearby emitters (such as atoms and molecules) in the evanescent-wave domain.

ACKNOWLEDGMENTS

The authors wish to acknowledge inspiring discussions with K. Busch. This work has received partial financial support from the People Programme (Marie Curie Actions) of the European Union's 7th Framework Programme FP7-PEOPLE-2011-IIF under REA grant agreement No. 302009 (Project HyPHONE), as well as from the Natural Sciences and Engineering Research Council of Canada (NSERC).

Appendix A: Fresnel's reflection coefficients in the evanescent-wave domain

In this Appendix, we would like to discuss the physical meaning of the Fresnel reflection coefficient at a plane interface between two media for such values of the in-plane component of the wave vector, κ , that the waves in one or both of the media can be evanescent. The goal is to understand which attributes of the complex reflection coefficient (real part, imaginary part, amplitude, and phase) have direct physical interpretation, and to show that this interpretation changes significantly when the incident wave is evanescent rather than propagating. We need this knowledge in order to elucidate the relation between the existence of propagating waves in the HMM structures and the non-zero imaginary part of the reflection coefficients introduced in the text in Eqs. (5), (7), (8), and (10)–(11), as well as through the transfer matrix calculation procedure.

We use the interface between two non-magnetic, isotropic media as an example, and begin by recalling the expression for the reflection coefficient for a p -polarized wave at such an interface,

$$r_{ij}(\kappa) = \frac{w_i(\kappa)\epsilon_j - w_j(\kappa)\epsilon_i}{w_i(\kappa)\epsilon_j + w_j(\kappa)\epsilon_i}, \quad (\text{A1})$$

assuming that there are no losses; therefore, we assume that $\epsilon_{i,j}$ are purely real (positive or negative), and, in turn, that $w_{i,j}$, defined in the same way as in Eq. (2), are both one of the following:

$$w_i(\kappa) \text{ is } \begin{cases} \text{real and positive,} & \epsilon_i > 0 \text{ and } \kappa < \frac{\omega}{c}\sqrt{\epsilon_i} \\ \text{positive imaginary,} & \text{otherwise.} \end{cases} \quad (\text{A2})$$

As mentioned in Section II, the first case corresponds to a wave that is propagating in medium i , whereas the second case corresponds to a wave that is evanescent in medium i . Depending on which of the cases of Eq. (A2) takes place for the two media (i and j) in Eq. (A1), four scenarios can be identified:

1. Both w_i and w_j are real, and hence r_{ij} is real. This is the usual Snell's refraction scenario: according to Eq. (A2), this is only possible if both ϵ_i and ϵ_j are non-negative so that the waves in both media are propagating, resulting in $|r_{ij}| < 1$, which means that the transmitted wave carries some of the incident energy away.
2. w_i is real but w_j is imaginary; the incident and reflected waves are propagating but the transmitted wave is evanescent. This is the total reflection scenario: either conventional total internal reflection on a dielectric-dielectric interface beyond the critical angle ($\sqrt{\epsilon_j} < \kappa c/\omega < \sqrt{\epsilon_i}$), or total reflection from a dielectric-metal interface ($\epsilon_j < 0 < \epsilon_i$). Here the reflection coefficient is of the form $(a - ib)/(a + ib)$ and therefore $|r_{ij}| = 1$, signifying that the transmitted evanescent wave transfers no energy away from the interface.
3. Both w_i and w_j are imaginary. Similar to #1 above, this means that r_{ij} must be real; however, $|r_{ij}|$ can be below or above unity depending on the signs of $\epsilon_{i,j}$. This is the scenario where all waves (incident, reflected, and transmitted) are evanescent, and no energy transfer through the interface occurs. If we were to change the medium i so as to support a propagating incident wave (e.g. by increasing its refractive index if it is a dielectric), this scenario would change to #2.
4. Finally, w_i is imaginary but w_j is real. Similar to #2 above, r_{ij} is of the form $(a - ib)/(a + ib)$ and therefore has an imaginary part. This is the "reversed total reflection" scenario when the incident and reflected waves are evanescent but the transmitted wave is *propagating*; if we were to change the medium i so as to support a propagating incident wave, this scenario would change to #1.

Suppose, now, that we know nothing about the nature of medium j beyond the interface and only treat that region as a "black box" (or the "sample"). We still know, and can choose, the medium i in front of the interface (the "cladding"), and we can perform some sort of ellipsometry-type reflectivity measurements on the interface. An important observation about the four scenarios listed above is that with the first two of them (#1 and #2), it is the *amplitude* of the reflection coefficient $|r_{ij}(\kappa)|$ that characterizes the sample's behavior at this particular κ ; we can conclude that $|r_{ij}| = 1$ means that there are no propagating waves in the sample (everything is totally reflected), and $|r_{ij}| < 1$ means that there are propagating waves in the sample. On the other hand, the *phase* of the reflection coefficient (or individually its real or imaginary part) cannot be attributed such physical significance. Indeed, adding a cladding layer of thickness d in front of the sample will not change anything in the physical system but will, according to Eqs. (10) and Fig. 2b, change $r_{ij}(\kappa)$ to $r'_{ij}(\kappa) = r_{ij}(\kappa)e^{2iw_i(\kappa)d}$, making its phase dependent on d and therefore, arbitrary.

On the other hand, if we apply the same line of reasoning to scenarios #3 and #4, we see that adding a similar cladding

layer of thickness d in front of the sample, with similar transformation $r_{ij}(\kappa) \rightarrow r'_{ij}(\kappa) = r_{ij}(\kappa)e^{2iw_i(\kappa)d}$, will change the *amplitude* rather than the phase of the reflection coefficient, since we are in the regime where w_i is imaginary; hence, it is $|r_{ij}|$ that can be made largely arbitrary. Therefore, it is now the *phase* of the reflection coefficient that characterizes the physics of the sample: $\arg r_{ij} \neq 0$ indicates that there are bulk propagating waves in the sample while $\arg r_{ij} = 0$ (real r_{ij}) unambiguously means that there are no such waves (although surface waves at the interface may still exist).

For practical purposes, whenever r_{ij} is non-zero, we can introduce a modified criterion based on the imaginary part of r_{ij} rather than on its phase. In these terms, $\text{Im}r_{ij} = 0$ (real r_{ij}) signifies the absence of bulk propagating waves in the sample, whereas $\text{Im}r_{ij} \neq 0$ indicates their presence, as confirmed in Fig. 3. We stress here that the magnitude of $\text{Im}r_{ij}$ still carries no direct physical significance in terms of characterizing the sample since $|r_{ij}|$ can be arbitrary; it is only whether it is zero or non-zero that is meaningful in the rigorous sense. However, we can relax our criterion somewhat, saying that $\text{Im}r_{ij} \approx 0$ implies the absence of propagating waves in the

sample, and significantly non-zero $\text{Im}r_{ij}$ implies their presence, as is demonstrated for the Bloch waves in Fig. 3b. Vague as the words “significantly non-zero” are, the criterion in this form was demonstrated to be useful in a broad range of parameters, including complex multilayers and lossy structures, as confirmed by calculating the field distribution at corresponding κ ; the only regime where we expect it to break down would be the case of high losses, where any non-arbitrary distinction between propagating and evanescent waves would be difficult.

We note, finally, that while the above analysis is carried out for an interface between two isotropic media, it remains valid if the sample is a homogenized HMM. Indeed, we see that Eq. (5) is essentially similar to Eq. (A1) as regards the applicability of Eq. (A2) and the subsequent reasoning; the sole reason for the explicit use of Eq. (A1) was to ease the explanation by being able to introduce a simple expression for w_j using ϵ_j . Moreover, as outlined in Section II in the discussion of Eq. (11), the reasoning remains applicable to more complex samples such as infinite (and to some extent, finite) multilayers.

-
- [1] J. Pendry, “Focus Issue: Negative refraction and metamaterials – Introduction,” *Opt. Express* 11(7), 639 (2003).
 - [2] M. Kuwata-Gonokami, N. Saito, Y. Ino, M. Kauranen, K. Jefimovs, T. Vallius, J. Turunen, and Y. Svirko, “Giant optical activity in quasi-two-dimensional planar nanostructures,” *Phys. Rev. Lett.* 95(22), 227401 (2005).
 - [3] D. R. Smith, D. Schurig, J. J. Mock, P. Kolinko, and P. Rye, “Partial focusing of radiation by a slab of indefinite media,” *Appl. Phys. Lett.* 84(13), 2244–2246 (2004).
 - [4] D. R. Smith, D. Schurig, and P. Kolinko, “Negative refraction in indefinite media,” *J. Opt. Soc. Am. B* 21(5), 1032–1043 (2004).
 - [5] A. Degiron, D. R. Smith, J. J. Mock, B. J. Justice, and J. Gollub, “Negative index and indefinite media waveguide couplers,” *Appl. Phys. A* 87(2), 321–328 (2007).
 - [6] W. Yan, L. Shen, L. Ran, and J. A. Kong, “Surface modes at the interfaces between isotropic media and indefinite media,” *J. Soc. Am. A* 24(2), 530–535 (2007).
 - [7] Z. Jacob, L. V. Alekseyev, and E. Narimanov, “Optical Hyperlens: Far-field imaging beyond the diffraction limit,” *Opt. Express* 14(18), 8247–8256 (2006).
 - [8] Z. Jacob, J.-Y. Kim, G. V. Naik, A. Boltasseva, E. E. Narimanov, and V. M. Shalaev, “Engineering photonic density of states using metamaterials,” *Appl. Phys. B* 100(1), 215–218 (2010).
 - [9] Z. Jacob, I. I. Smolyaninov, and E. E. Narimanov, “Broadband Purcell effect: Radiative decay engineering with metamaterials,” *Appl. Phys. Lett.* 100(18), 181105 (2012).
 - [10] C. Simovski, S. Maslovski, I. Nefedov, and S. Tretyakov, “Optimization of radiative heat transfer in hyperbolic metamaterials for thermophotovoltaic applications,” *Opt. Express* 21(12), 14988–15013 (2013).
 - [11] I. I. Smolyaninov and Yu-Ju Hung, “Modeling of time with metamaterials,” *J. Opt. Soc. Am. B* 28(7), 1591–1595 (2011).
 - [12] I. I. Smolyaninov and E. E. Narimanov, “Metric signature transitions in optical metamaterials,” *Phys. Rev. Lett.* 105(6), 067402 (2010).
 - [13] M. A. Noginov, Yu. A. Barnakov, G. Zhu, T. Tumkur, H. Li, and E. E. Narimanov, “Bulk photonic metamaterial with hyperbolic dispersion,” *Appl. Phys. Lett.* 94(15), 151105 (2009).
 - [14] M. A. Noginov, H. Li, Yu. A. Barnakov, D. Dryden, G. Nataraj, G. Zhu, C. E. Bonner, M. Mayy, Z. Jacob, and E. E. Narimanov, “Controlling spontaneous emission with metamaterials,” *Opt. Lett.* 35(11), 1863–1865 (2010).
 - [15] J. Kanungo and J. Schilling, “Experimental determination of the principal dielectric functions in silver nanowire metamaterials,” *Appl. Phys. Lett.* 97(2), 021903 (2010).
 - [16] C. L. Cortes, W. Newman, S. Molesky, and Z. Jacob, “Quantum nanophotonics using hyperbolic metamaterials,” *J. Opt.* 14, 063001 (2012).
 - [17] V. Drachev, V. A. Podolskiy, and A. V. Kildishev, “Hyperbolic Metamaterials: new physics behind a classical problem,” *Opt. Express* 21, 15048–15064 (2013).
 - [18] O. Kidwai, S. V. Zhukovsky, and J. E. Sipe, “Dipole radiation near hyperbolic metamaterials: applicability of effective-medium approximation,” *Opt. Lett.* 36(13), 2530–2532 (2011).
 - [19] I. Iorsh, A. Poddubny, A. Orlov, P. Belov, and Yu. Kivshar, “Spontaneous emission enhancement in metal-dielectric metamaterials,” *Phys. Lett. A* 376(3), 185–187 (2012).
 - [20] I. Avrutsky, I. Salakhutdinov, J. Elser, and V. Podolskiy, “Highly confined optical modes in nanoscale metal-dielectric multilayers,” *Phys. Rev. B* 75(24), 241402(R) (2007).
 - [21] S. Ishii, A. V. Kildishev, E. Narimanov, V. M. Shalaev, and V. P. Drachev, “Sub-wavelength interference pattern from volume plasmon polaritons in a hyperbolic medium,” *Laser Photon. Rev.* 7(2), 365–271 (2013).
 - [22] S. Feng, J. M. Elson, and P. L. Overfelt, “Optical properties of multilayer metal-dielectric nanofilms with all-evanescent modes,” *Opt. Express* 13(11), 4113–4124 (2005).
 - [23] G. Rosenblatt and M. Orenstein, “Competing coupled gaps and slabs for plasmonic metamaterial analysis,” *Opt. Express* 19(21), 20372–20385 (2011).
 - [24] J. Schilling, “Uniaxial metallo-dielectric metamaterials with scalar positive permeability,” *Phys. Rev. E* 74(4), 046618 (2006).
 - [25] J. Elser, V. A. Podolskiy, I. Salakhutdinov, and I. Avrutsky,

- “Nonlocal effects in effective-medium response of nanolayered metamaterials,” *Appl. Phys. Lett.* 90(19), 191109 (2007).
- [26] S. V. Zhukovsky, O. Kidwai, and J. E. Sipe, “Physical nature of volume plasmon polaritons in hyperbolic metamaterials,” *Opt. Express* 21, 14982 (2013).
- [27] J. J. Saarinen and J. E. Sipe, “A Green function approach to surface optics in anisotropic media,” *J. Mod. Opt.* 55(1), 13–32 (2008).
- [28] O. Kidwai, S. V. Zhukovsky, and J. E. Sipe, “Effective-medium approach to planar multilayer hyperbolic metamaterials: Strengths and limitations,” *Phys. Rev. A* 85(5), 053842 (2012).
- [29] A. Yariv and P. Yeh, *Optical Waves in Crystals* (New York: Wiley, 1983).
- [30] X. Ni, S. Ishii, M. Thoreson, V. Shalaev, S. Han, S. Lee, and A. Kildishev, “Loss-compensated and active hyperbolic metamaterials,” *Opt. Express* 19(25), 25242–25254 (2011).
- [31] S. V. Zhukovsky, “Perfect transmission and highly asymmetric light localization in photonic multilayers,” *Phys. Rev. A* 81(5), 053808 (2010).
- [32] S. V. Zhukovsky, L. G. Helt, D. Kang, P. Abolghasem, A. S. Helmy, and J. E. Sipe, “Analytical description of photonic waveguides with multilayer claddings: Towards on-chip generation of entangled photons and Bell states,” *Opt. Commun.* 301–302, 127–140 (2013).
- [33] P. R. West, S. Ishii, G. V. Naik, N. K. Emani, V. M. Shalaev, and A. Boltasseva, “Searching for better plasmonic materials,” *Laser Photon. Rev.* 4(6), 795–808 (2010).
- [34] A. N. Poddubny, P. A. Belov, and Yu. S. Kivshar, “Spontaneous radiation of a finite-size dipole emitter in hyperbolic media,” *Phys. Rev. A* 84(2), 023807 (2011).
- [35] E. Maciá, “The role of aperiodic order in science and technology,” *Rep. Prog. Phys.* 69(2), 397–441 (2006).
- [36] X. Sun and D. Jaggard, “Wave interactions with generalized Cantor bar fractal multilayers,” *J. Appl. Phys.* 70(5), 2500–2507 (1991).
- [37] C. Sibilia, I. S. Nefedov, M. Scalora, and M. Bertolotti, “Electromagnetic mode density for finite quasi-periodic structures,” *J. Opt. Soc. Am. B* 15(7), 1947–1952 (1998).
- [38] A. V. Lavrinenko, S. V. Zhukovsky, K. S. Sandomirskii, and S. V. Gaponenko, “Propagation of classical waves in nonperiodic media: Scaling properties of an optical Cantor filter,” *Phys. Rev. E* 65(3), 036621 (2002).
- [39] S. V. Zhukovsky, A. V. Lavrinenko, and S. V. Gaponenko, “Spectral scalability as a result of geometrical self-similarity in fractal multilayers,” *Europhys. Lett.* 66(3), 455–461 (2004).
- [40] S. V. Zhukovsky and A. V. Lavrinenko, “Spectral self-similarity in fractal one-dimensional photonic structures,” *Photonics and Nanostructures – Fundamentals and Applications* 3(2–3), 129–133 (2005).